Applied Surface Science 366 (2016) 455–463

Contents lists available at ScienceDirect

Applied Surface Science

journal homepage: www.elsevier.com/locate/apsusc

Sulfur passivation for the formation of Si-terminated Al_2O_3/SiGe(0 0 1) interfaces

Kasra Sardashti[a,b], Kai-Ting Hu[a,c], Kechao Tang[d], Sangwook Park[a,b], Hyonwoong Kim[a,b], Shailesh Madisetti[e], Paul McIntyre[d], Serge Oktyabrsky[e], Shariq Siddiqui[f], Bhagawan Sahu[f], Noami Yoshida[g], Jessica Kachian[g], Andrew Kummel[a,*]

[a] Department of Chemistry and Biochemistry, University of California, San Diego, La Jolla, CA, United States
[b] Materials Science and Engineering Program, University of California, San Diego, La Jolla, CA, United States
[c] Department of Mechanical and Aerospace Engineering, University of California, San Diego, La Jolla, CA, United States
[d] Department of Materials Science and Engineering, Stanford University, CA, United States
[e] Department of Nanoscale Science and Engineering, University at Albany—State University of New York, Albany, NY, United States
[f] TD Research, GLOBALFOUNDRIES USA, Inc., Albany, NY, United States
[g] Applied Materials, Inc., Santa Clara, CA, United States

ARTICLE INFO

Article history:
Received 9 September 2015
Received in revised form
13 December 2015
Accepted 14 January 2016
Available online 16 January 2016

Keywords:
Silicon–germanium
Sulfur passivation
Atomic layer deposition
Aluminum oxide

ABSTRACT

Sulfur passivation is used to electrically and chemically passivate the silicon–germanium (SiGe) surfaces before and during the atomic layer deposition (ALD) of aluminum oxide (Al_2O_3). The electrical properties of the interfaces were examined by variable frequency capacitance–voltage (*C–V*) spectroscopy. Interface compositions were determined by angle-resolved X-ray photoelectron spectroscopy (AR-XPS). The sulfur adsorbs to a large fraction of surface sites on the SiGe(0 0 1) surface, protecting the surface from deleterious surface reactions during processing. Sulfur passivation (a) improved the air stability of the cleaned surfaces prior to ALD, (b) increased the stability of the surface during high-temperature deposition, and (c) increased the Al_2O_3 ALD nucleation density on SiGe, thereby lowering the leakage current. S passivation suppressed formation of Ge—O bonds at the interface, leaving the majority of the Al_2O_3–SiGe interface terminated with direct Si—O—Al bonding.

Published by Elsevier B.V.

1. Introduction

The demand for scaling complementary metal–oxide–semiconductor (CMOS) technology necessitates the application of thinner high-k dielectrics and channel materials with higher electron or hole mobility in combination with novel device architectures, such as fin field effect transistors (FinFETs) and nanowire field effect transistors (NW-FETs) [1,2]. In contrast to some other high-mobility channel materials, such as Ge or III-V compounds, silicon-germanium (SiGe) alloys offer the tunability of band gaps and carrier mobilities through variations in the Ge content and subsequent tensile/compressive stresses [3]. In addition, compared to other potential channel materials, SiGe alloys can be more easily integrated into a Si CMOS process flow and have a relatively mature device fabrication technology, owing to its application in high-speed heterojunction bipolar transistors (HBTs) [4]. Controlling the interface quality between high-k dielectrics and SiGe alloys, particularly in nanoscale devices such as FinFETs, is the key to the integration of these materials into future CMOS technology.

To develop high-performance SiGe FETs, high-k dielectrics should be used as gate dielectrics. Therefore, it is vital to reduce the density of the interface and near-interface traps between the high-k gate oxide and SiGe channel layer [5]. The presence of Ge at the surface and within the native oxide makes high-k/SiGe interface passivation challenging because of GeO_2 water solubility and reliability issues caused by Ge out-diffusion through the gate oxide [6]. High-k/semiconductor interface passivation has been extensively studied for various semiconductors, such as Ge, III-V compounds (i.e. GaAs, InGaAs, etc.) and III-N (i.e. GaN). Interface passivation can be achieved either by wet ex situ or dry in situ clean depending on the composition of passivating species and the physical form of their precursors. Sulfur passivation using wet ex situ $(NH_4)_2S$ dip[7] or in situ H_2S exposure[8] has been used to passivate semiconductor surface defects or trapping sites by forming —S covalent bonds to the substrate atoms. Ex situ S passivation

* Corresponding author.
E-mail address: akummel@ucsd.edu (A. Kummel).

http://dx.doi.org/10.1016/j.apsusc.2016.01.123
0169-4332/Published by Elsevier B.V.

has been successfully applied to a wide range of semiconductors, including GaAs [9], InGaAs [10], GaN [11], and Ge [7], to improve the quality of their interfaces with high-k gate dielectrics, such as aluminum oxide (Al_2O_3), HfO_2, HfON, etc. For Ge(0 0 1), S passivation results in a smaller equivalent oxide thickness (EOT), a smaller density of the interface traps, and the reduction of Ge—O bonding at the interface by passivating the Ge dangling bonds via the formation of Ge—S, Ge—S—Ge, or Ge—SH bonds, depending on whether dry or wet processing is employed [12–14]. Considering the presence of Ge atoms on the SiGe surface, S passivation can be an efficient method of high-k/SiGe interface passivation.

This study determines the effect of S passivation by ex situ $(NH_4)_2S$ cleaning on the interface composition and electrical characteristics of Al_2O_3/SiGe(0 0 1). Al_2O_3 was deposited on SiGe at 120, 200, and 300 °C using atomic layer deposition (ALD). The electrical properties of the $Al_2O_3/Si_{0.7}Ge_{0.3}$(1 0 0) interfaces were characterized by capacitance–voltage (*C–V*) and current–voltage (*I–V*) measurements on metal oxide semiconductor (MOS) capacitors. The chemical compositions of the oxide/SiGe interfaces for different ALD temperatures in the presence or absence of $(NH_4)_2S$ cleaning were determined by angle resolved X-ray photoelectron spectroscopy (AR-XPS). S passivation strongly prevented the formation of Ge—O interface bonding and assisted in the formation of direct Si—O—Al bonding between Al_2O_3 and SiGe.

2. Experimental details

A 12-nm-thick p-type $Si_{0.7}Ge_{0.3}$(1 0 0) with a doping level of 1×10^{18} cm^{-3} (Applied Materials) was grown epitaxially on p-type Si(1 0 0) by molecular beam epitaxy (MBE). No Si or Ge capping layer was deposited on the wafers following SiGe growth. Al_2O_3–SiGe metal–oxide–semiconductor capacitors (MOSCAPs) were fabricated through the ALD deposition of Al_2O_3 followed by 50-nm Ni gate deposition via thermal evaporation and 100-nm Al back contact deposition using DC sputtering. Prior to ALD, organic cleaning (30 s rinse by each of acetone, isopropyl alcohol, and DI H_2O solutions followed by N_2 drying) was followed by native oxide removal via cyclic HF cleaning using a 2% HF solution and DI water at 25 °C for 1 min in each solution for 2.5 cycles, ending with the HF dip. For ex situ S passivation, samples were dipped for 30 min in a 25% $(NH_4)_2S$ solution at 25ºC. The S passivation recipe has been optimized by investigating the MOSCAP characteristics as functions of $(NH_4)_2S$ exposure time and the solution temperature (Supporting information, Fig. S1). To deposit thin Al_2O_3 using ALD, samples were transferred to the ALD chamber with minimal exposure to air (maximum 2 min). ALD was performed at 120, 200, and 300 °C in a Beneq TFS-200 continuous flow reactor with Ar as the carrier gas. The Al_2O_3 deposition started with 20 cycles of 45 ms Trimethylaluminum (TMA) pulses, followed by 30 consecutive cycles of 200 ms of TMA and 50 ms of H_2O. After each TMA and H_2O pulse, a 6-s Ar purge was employed. The chamber pressure during the ALD process was 1.7 Torr. The deposition rate determined by ellipsometry on a Si(100) monitor sample with 10, 50, and 100 nm of Al_2O_3 was 1.03 A/cycle. Therefore, the oxide thickness is estimated as 3.1 nm. This thickness estimation is subjected to uncertainties due the differences in the substrate used, as well as a larger thickness measured for ellipsometry. After fabrication, MOSCAPs were annealed in forming gas (5% H_2, 95% N_2) at 250 °C for 15 min. Details of the forming gas anneal optimization are given in the supporting information (Fig. S2).

C–V spectroscopy of the MOSCAPs was performed using an Agilent B-1500 semiconductor analyzer with an AC modulation amplitude of 30 mV in the gate bias range of −2 to 2 V at multiple frequencies, from 2 KHz to 1 MHz. Using the capacitance and conductance vs. gate voltage, the densities of the interface traps were calculated using the full interface state model with the Δ circuit of three complex elements method [15], and the density of the border traps (N_{bt}) was extracted by Taur's model, assuming a spatially uniform trap distribution [16]. Gate leakage vs. gate bias was measured in the same bias range. To determine the composition of the $Al_2O_3/Si_{0.7}Ge_{0.3}$(0 0 1) interfaces as a function of the surface preparation method, AR-XPS and near-normal angle XPS were performed on SiGe samples after eight cycles of Al_2O_3 ALD. AR-XPS measurements were performed by a VG Theta Probe system using an Al-Kα excitation source (1486.7 eV). Si2p, Ge2p, Ge3d, Al2p, S2p, and O1s spectra were obtained at various take-off angles, starting from 26.75° to 79.25° with 7.5° steps. Near-normal angle XPS was performed using a monochromatic XM 1000 MkII/SPHERA (by Omicron Nanotechnology) XPS system with an Al-Kα source (E = 1486.7 eV). For all measurements, a take-off angle of 30° from the sample surface was used.

3. Results and discussion

The effects of surface passivation on the electrical properties of Al_2O_3/SiGe interfaces were determined by *C–V* spectroscopy on the MOSCAPs. Fig. 1 shows the variable frequency *C–V* results at 2 kHz to 1 MHz for the samples with no surface cleaning (except organic cleaning to remove organic contaminants), HF only, and HF + $(NH_4)_2S$ treatments followed by Al_2O_3 ALD at 120 and 300 °C. Compared with the samples with no surface cleaning (a, d), both HF (b, e) and HF + $(NH_4)_2S$ (c, f) increased the maximum capacitance achieved in accumulation by removing the SiGe native oxide and reducing the total oxide thickness. For cleaned surfaces, increasing the ALD temperature from 120 to 300 °C resulted in a larger frequency dispersion at negative gate biases, where majority carrier (hole) accumulation occurs. This dispersion corresponds to the border traps, which are trap states located within the oxide layer near the interface with energy levels adjacent to the majority carrier band [17]. Similarly, the height of the low-frequency "bump" that appears in the *C–V* curves between 0 and +0.5 V corresponds to the density of the interface trap states [12,18]. While 300 °C ALD in the presence of native oxide resulted in a dramatic increase in the interface trap capacitance, for S-passivated surfaces, this change was fairly small.

Fig. 2 displays the density of the interface traps (D_{it}) as a function of the Fermi level position relative to the valence band edge, as extracted from the *G–V* characteristics of the devices shown in Fig. 1. Regardless of the surface preparation method, the largest densities of interface traps are concentrated at 0.25–0.4 eV above the valence band edge. Such a defect energy distribution is identical to the ones reported for Si dangling bond P_b centers at the SiO_2/Si interfaces, which is consistent with the formation of Si—O—Al at the interface between SiGe and Al_2O_3 [19–24]. For HF-cleaned surfaces, increasing the ALD temperature to 300 °C results in a 5×10^{12} eV^{-1} cm^{-2} maximum density of interface traps, as opposed to only a 4×10^{12} eV^{-1} cm^{-2} maximum density for S-passivated surfaces. It is noted that at 120 °C, the D_{it} is nearly identical for both surface treatments, while the 300 °C results are consistent with S providing additional protection of the surface from unwanted reactions, such as substrate oxidation at an elevated temperature.

Additional electrical parameters derived from the variable frequency *C–V* measurements, including EOT, density of border traps (N_{bt}), and flat band voltage (V_{FB}), are listed in Table 1. N_{bt} is extracted at a surface energy of $E - E_v = -0.22$ eV. For comparison, N_{bt} and V_{FB} for ALD at 120 °C for samples with only organic solvent cleaning were included. Compared to the sample with no cleaning, HF cleaning and S passivation reduced the EOT by 35–40% to 2.1–2.25 nm, with the S-passivated sample having the

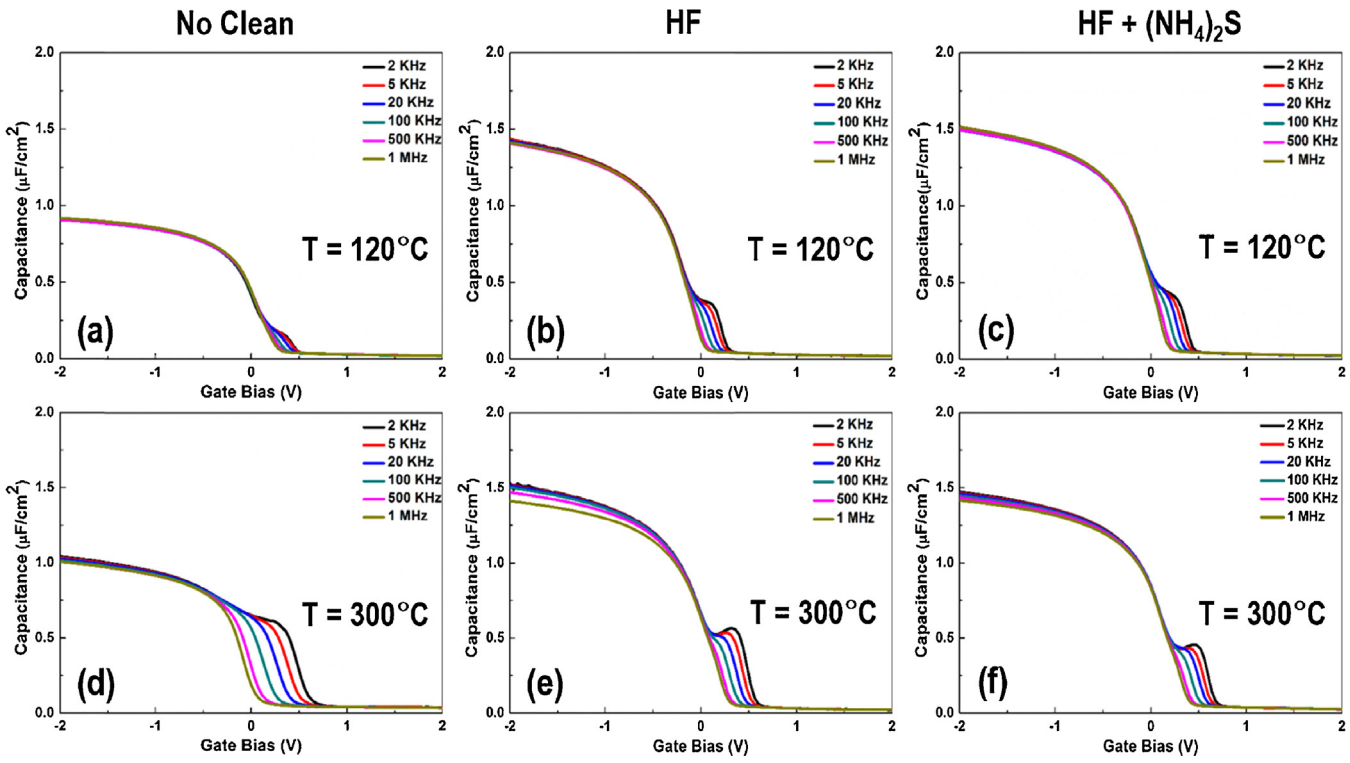

Fig. 1. Multi-frequency *C–V* measurements for Al_2O_3 on SiGe with no surface cleaning (a and d), HF surface treatment (b and e), and S passivation (c and f). Al_2O_3 ALD for (a–c) was performed at 120 °C and it was performed at 300 °C for (d–f).

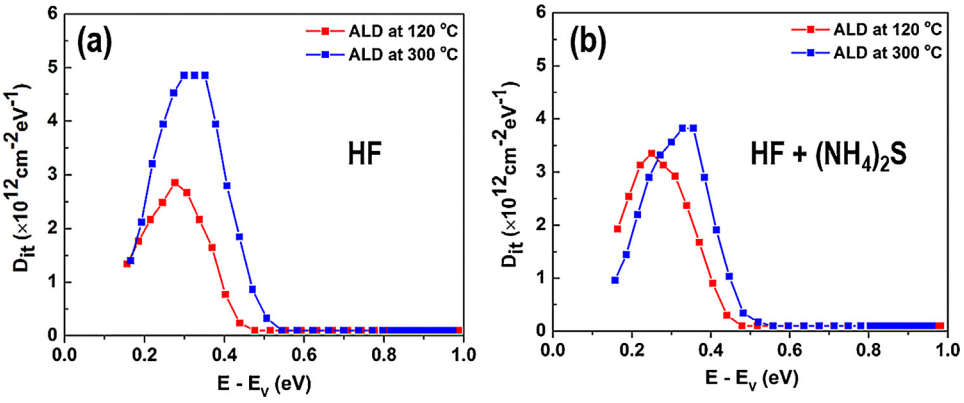

Fig. 2. The density of the interface trap as a function of energy relative to the valence band edge for (a) HF-treated and (b) S-passivated Al_2O_3/SiGe interfaces with ALD performed at 120 and 300 °C.

smallest EOT, at 2.09 nm. Consistent with a qualitative assessment of the *C–V* measurements in the accumulation region, a higher temperature for both cleaning methods doubles the density of the border traps. However, this difference could be partially due to the higher series resistance that increases the errors in the border trap calculations. In addition, higher ALD temperatures resulted in a 0.2–0.25 V shift in the flat band voltage for both samples. In sum, S passivation compared to the HF treatment resulted in a slightly smaller EOT (which could be due to thinner interfacial oxide and a higher equivalent dielectric constant), but the ALD at 120 °C was

Table 1
Parameters extracted from the *C–V* measurements on SiGe samples with no cleaning, HF treatment, and S passivation. All standard errors are included. It is noted that the reported N_{bt} for the 300 °C sample may be increased in part by series resistance, even though this was incorporated into the model.

	No cleaning	HF		HF + $(NH_4)_2S$	
Parameter/temperature	120 °C	120 °C	300 °C	120 °C	300 °C
EOT (nm)	3.49 (±0.17)	2.23 (±0.1)	2.13 (±0.1)	2.09 (±0.1)	2.23 (±0.1)
N_{bt} ($\times 10^{19}$ cm^{-3} eV^{-1})	7.0 (±0.55)	6.2 (±0.5)	10.0 (±0.5)	5.8 (±0.5)	11.0 (±0.5)
V_{FB} (V)	0.10 (±0.01)	−0.05 (±0.01)	0.14 (±0.01)	0.10 (±0.04)	0.35 (±0.04)
D_{it} ($\times 10^{12}$ cm^{-2} eV^{-1})	0.6 (±0.1)	1.7 (±0.2)	3.2 (±0.2)	2.0 (±0.2)	2.5 (±0.2)
Q_{ox} ($\times 10^{12}$ cm^{-2})	−0.69 (±0.06)	+0.37 (±0.06)	−1.5 (±0.19)	−1.13 (±0.13)	−2.69 (±0.31)

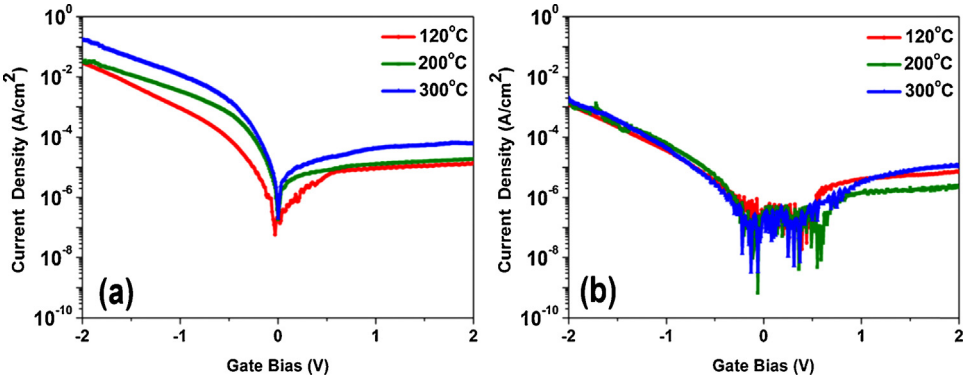

Fig. 3. Leakage current vs. gate bias for ALD-Al_2O_3 with a deposition temperature of 120, 200, and 300 °C on (a) HF-treated and (b) S-passivated SiGe surfaces.

shown to be beneficial regardless of the surface treatment in terms of a lower density of interface and border traps.

Gate leakage currents (I_g–V_g) for the two ALD temperatures with different surface passivation conditions were determined, as shown in Fig. 3. For HF-cleaned samples, raising the temperature to 300 °C increases the maximum leakage current in depletion (V_g = 2 V) as well as in accumulation (at V_g = −2 V) by an order of magnitude. This is consistent with a decrease in the EOT by increasing the ALD temperature for HF-cleaned surfaces. In contrast, the leakage current for S-passivated interfaces is independent of the ALD temperature at almost all gate biases. In addition, the maximum leakage current in accumulation for S-passivated SiGe surfaces is one to two orders of magnitude smaller than the one for HF-treated surfaces with ALD at 120 °C to 300 °C. The gate leakage characteristics of S-passivated samples can be ascribed to the higher density and higher uniformity of Al_2O_3 nucleation on these surfaces, as opposed to H-terminated surfaces [25].

An air-stable passivated surface enables the transfer of wet cleaned wafers in ambient without decreasing the interface quality [26]. To determine the air stability, clean SiGe surfaces after HF and S treatments were exposed to air for 30 and 60 min prior to insertion into the ALD reactor and subsequent Al_2O_3 deposition. Fig. 4 displays the C–V characteristics of the Al_2O_3–SiGe MOSCAPs fabricated with air-exposed samples. For comparison, C–V measurements for samples with minimal air exposure (~2 min), as shown in Fig. 1, are displayed again, as in Fig. 4a and d. Qualitatively, the frequency dispersion of the C–V curves displays no change between the two surface preparation conditions as a function of air exposure. The D_{it} calculations shown in Fig. 5 suggest that air exposure for both HF-cleaned and S-passivated samples caused a ~30% increase in the maximum D_{it}. However, the HF-cleaned sample showed a 0.7×10^{12} eV^{-1} cm^{-2} lower D_{it} than S-passivated samples for long air exposures.

The EOT, N_{bt}, and V_{FB} values for samples exposed to air between cleaning and ALD are listed in Table 2. For both H- and S-passivated surfaces, the EOT showed only 5% variations. Similar to the observation of EOT vs. ALD temperature, S-passivated Al_2O_3/SiGe interfaces have a lower EOT than HF-cleaned surfaces. For both passivation techniques, the N_{bt} levels varied by small amounts with longer air exposure times. However, the main advantage of

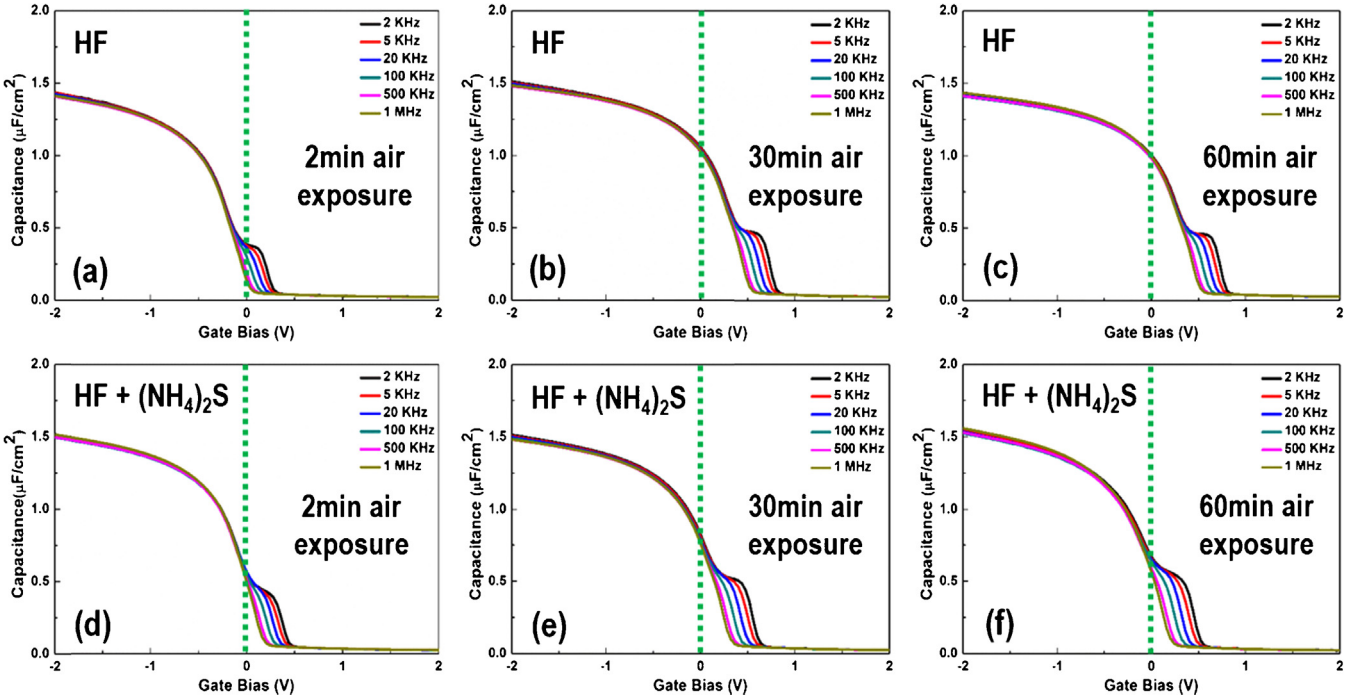

Fig. 4. Multi-frequency C–V measurements for Al_2O_3 on SiGe with 2, 30, and 60 min of air exposure between wet cleaning and Al_2O_3 ALD for (a–c) HF-treated and (d–f) S-passivated surfaces prior to ALD. The green dotted line indicates the zero gate bias.

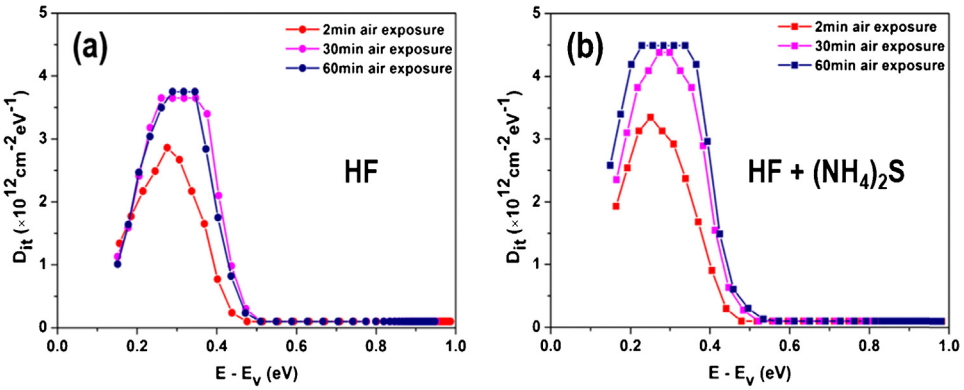

Fig. 5. The density of the interface trap as a function of energy relative to the valence band edge for (a) HF-treated and (b) S-passivated Al_2O_3/SiGe interfaces with 2, 30, and 60 min of air exposure between wet cleaning and ALD.

Table 2
Parameters extracted from the *C–V* measurements on SiGe samples with HF treatment and S passivation for 2, 30, and 60 min of air exposure prior to Al_2O_3 ALD. All standard errors are included.

	HF			HF + $(NH_4)_2S$		
Parameter/air exposure	2 min	30 min	60 min	2 min	30 min	60 min
EOT (nm)	2.23 (±0.1)	2.09 (±0.1)	2.20 (±0.1)	2.09 (±0.1)	2.10 (±0.1)	2.00 (±0.1)
N_{bt} ($\times 10^{19}$ cm^{-3} eV)	6.2 (±0.5)	5.5 (±0.5)	6.2 (±0.5)	5.8 (±0.5)	6.5 (±0.5)	6.6 (±0.5)
V_{FB} (V)	−0.05 (±0.01)	0.40 (±0.01)	0.40 (±0.01)	0.10 (±0.04)	0.22 (±0.04)	0.12 (±0.04)
D_{it} ($\times 10^{12}$ cm^{-2} eV^{-1})	1.7 (±0.2)	2.7 (±0.2)	2.6 (±0.2)	2.0 (±0.2)	3.0 (±0.3)	3.3 (±0.3)
Q_{ox} ($\times 10^{12}$ cm^{-2})	+0.37 (±0.06)	−4.25 (±0.50)	−4.00 (±0.50)	−1.13 (±0.13)	−2.31 (±0.19)	−1.56 (±0.19)

S passivation is the stability of the flat band voltage and oxide total charge (Q_{ox}). For HF-cleaned samples, after 30 or 60 min of exposure to air, V_{FB} shifted by 450 mV (more than a 3.75×10^{12} cm^{-2} increase in negative charge). Conversely, S-passivated interfaces maintained a nearly constant V_{FB} (<120 mV variation) with a maximum 1.25×10^{12} cm^{-2} increase in Q_{ox}. Large V_{FB} and Q_{ox} shifts can adversely affect device performance by largely changing the threshold voltage of the resulting devices [27]. Therefore, S passivation can be a promising surface preparation method for SiGe wafers in FET fabrication by extending the queue time by up to an hour.

The gate leakage current characteristics vs. air exposure time prior to ALD were evaluated, as illustrated in Fig. 6. The leakage current for HF-cleaned surfaces in accumulation increased more than an order of magnitude by exposing samples to air for 30 or 60 min (Fig. 6a). Conversely, the leakage currents for S-passivated samples at all gate biases had nearly zero change as a function of surface air exposure prior to ALD. Exposure to air increased the absolute difference between the gate leakage currents of HF-cleaned and S-passivated samples to more than two orders of magnitude.

To determine the role of surface passivation in the chemical bonding changes at the Al_2O_3–SiGe interface, Si2p, Ge3d, and Ge2p peaks were collected by AR-XPS over a range of take-off angles, as shown in Fig. 7. To prevent a strong attenuation of the SiGe substrate signals by the Al_2O_3 layer, only eight cycles of ALD, equivalent to a 0.8-nm thickness, were deposited on the samples at 120 °C. No post-deposition anneal (PDA) after ALD was performed on the samples shown in Fig. 7. The peak decomposition has been performed for Si2p, Ge3d, and Ge2p according to Refs. [28] and [29]. The Si2p peaks (Fig. 7a and b) for HF-treated and S-passivated interfaces show a shoulder between 101.5 eV and 102.5 eV at all take-off angles that correspond to SiO_x (SiO and Si_2O_3) rather than stoichiometric SiO_2. This is consistent with the formation of Si—O bonds at the interface. Similarly, Ge3d peaks (Fig. 7c and d) show shoulders at 32 eV associated with GeO_x (GeO and Ge_2O_3). However, S passivation resulted in a significant increase in the SiO_x-to-GeO_x ratio

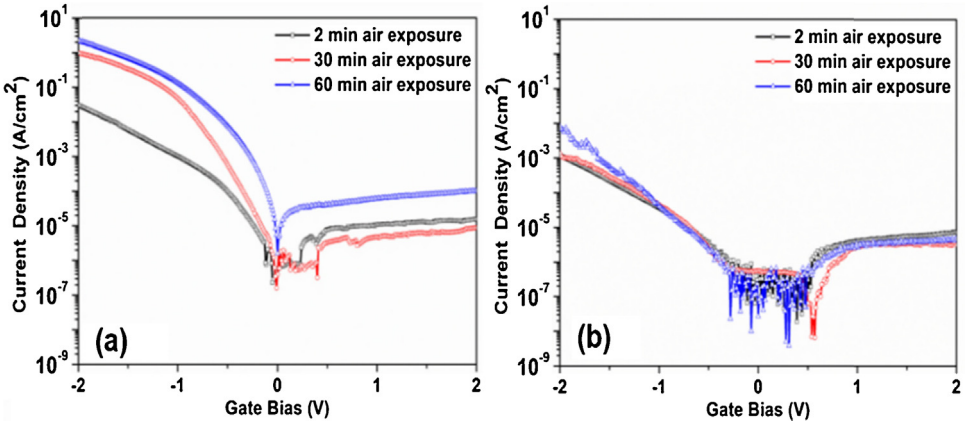

Fig. 6. Leakage current vs. gate bias for ALD-Al_2O_3 deposited at 120 °C on (a) HF-treated and (b) S-passivated SiGe surfaces with 2, 30, and 60 min of air exposure before oxide deposition.

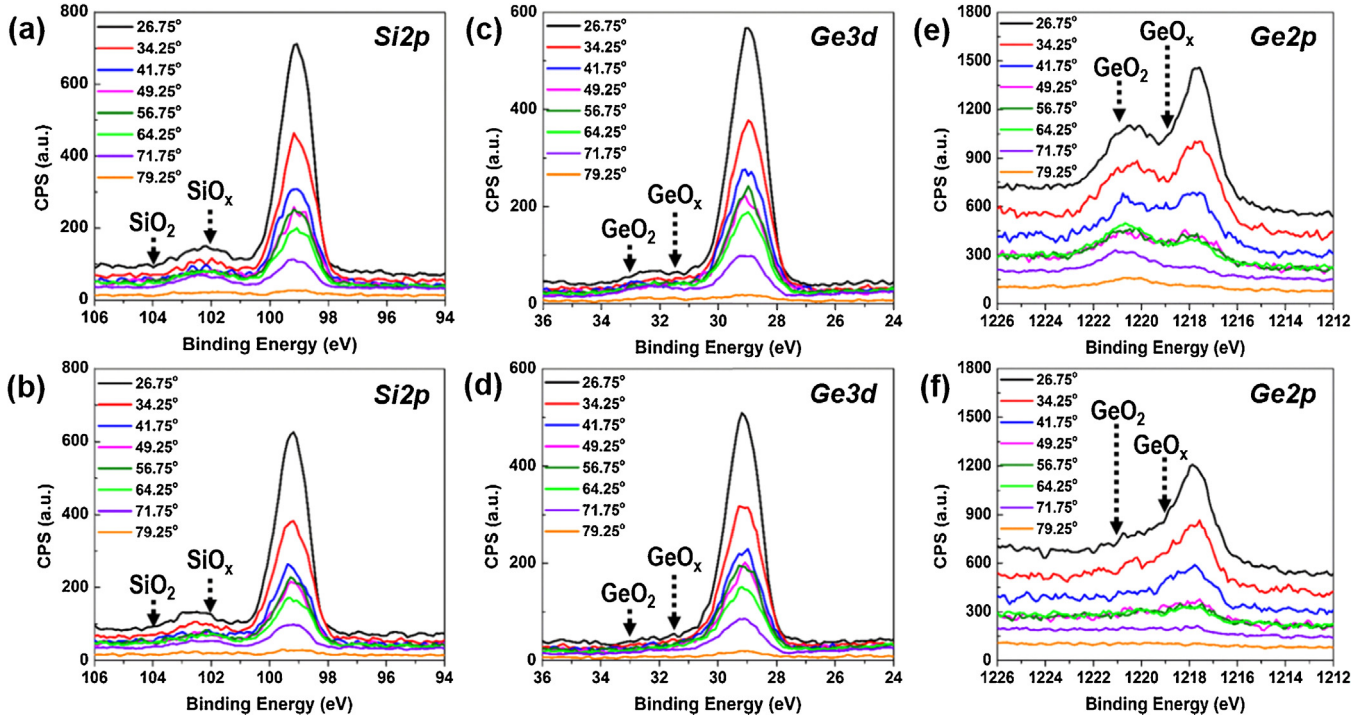

Fig. 7. Si2p (a and b), Ge3d (c and d), and G2p (e and f) spectra as functions of the photoelectron take-off angle for SiGe surfaces with 0.8 nm of ALD-Al_2O_3 on top, deposited at 120 °C. (a), (c), and (e) show the spectra for HF-treated interfaces, while (b), (d), and (f) display those for S-passivated interfaces. Note: neither FGA nor PDA was performed on these samples.

at the interface (from 1.3 for HF-treated to 2.23 for S-passivated surfaces), leaving the Al_2O_3–SiGe interface almost exclusively terminated with Si—O—Al rather than Ge—O—Al bonds (details of the Ge3d peak decomposition are shown in Fig. S3). For S-passivated samples, it can also be hypothesized that a fraction of Si atoms at the interface forms Si—S—Al bonds. However, this cannot be quantified due to the overlap between Si—O and Si—S peak positions in the S2p spectrum. Due to the propensity to form H_2S in the presence of atomic hydrogen, S is expected to be removed from the interface upon forming gas annealing.

In the case of Ge2p peaks, the difference between the intensity of the high-binding shoulder for HF-treated and S-passivated interfaces is more pronounced. The shoulders in Ge2p (Fig. 7e) for HF-treated SiGe surfaces are associated with the presence of sub-stoichiometric GeO_x and stoichiometric GeO_2. The GeO_2 component has strongly been reduced by S passivation, leaving mostly peaks for Ge—O bonds behind (Fig. 7f). It should be noted that Ge2p photoelectrons have a lower kinetic energy with an inelastic mean-free path (IMFP) of 0.85 nm, which makes them very surface-sensitive [30]. Due to the 0.8-nm-thick Al_2O_3 surface layer, a large portion of the Ge2p signal might originate from the interior of the oxide or oxide surface. Therefore, the observation of a broad high-binding-energy shoulder for Ge2p peaks in Fig. 7e, particularly at grazing angles, such as 71.75° and 79.25°, is consistent with the presence of GeO_x ($x \leq 2$) within or on top of the oxide. This high-binding energy peak is significantly suppressed for S-passivated surfaces at both 120 and 300 °C ALD temperatures (Fig. 7f, Supplemental materials Fig. S4). Ge out-diffusion and its incorporation into the high-k gate dielectrics is commonly observed and known to lower device reliability and increase gate leakage [31,32]. A similar experiment was repeated with 16 cycles of Al_2O_3 ALD, where trace amounts of the Ge2p signal were detected only at the most normal take-off angle of 26.75° (Fig. S5), confirming that Ge out-diffusion from SiGe within Al_2O_3 is limited to the first 0.8–1.0 nm of the oxide adjacent to the Al_2O_3/SiGe interface for deposition temperatures as low as 120 °C (with the assumption that the Ge 2p effective attenuation length [EAL] is less than 8.5 nm). Ge out-diffusion could occur during or after the ALD process, where Ge diffuses into the growing Al_2O_3 monolayer and moves with the growing layers to the top surface. It is also possible that Ge diffuses through the first few monolayers of the oxide when the last layers are grown (particularly in the case of 1.6-nm-thick oxide). Ge out-diffusion might also occur within the first few monolayers of Al_2O_3, while the sample is kept at 120 °C before removal from the ALD chamber. Accordingly, S passivation significantly reduced the Ge—O bonds at the interface and prevented Ge incorporation into the oxide, improving the interface quality.

To reproduce the forming gas anneal conditions, it is necessary to supply atomic hydrogen to the interface. For MOSCAPs, the Ni gate provides atomic H by catalyzing the reaction: $H_2 \rightarrow 2H^*$ [33]. However, performing XPS in the presence of metallic gates is challenging, particularly for 0.8-nm-thick oxides. Therefore, to simulate the forming gas annealing conditions for S-passivated SiGe surfaces, five cycles of TMA and H_2O were dosed on the SiGe surface in UHV at 120 °C followed by annealing at 300 °C for 20 min and a 500-Langmuir atomic H dose at 330 °C (500 s at 1×10^{-6} Torr). After each of these processing steps, the surface composition was measured using in situ XPS at a 30° take-off angle (more normal angle).

Fig. 8 displays the Si2p, Ge3d, and Ge2p peaks at the four different processing steps, including S passivation (as-received), a 0.5-nm Al_2O_3 deposition, UHV annealing at 300 °C, and atomic H dosing on the sample at 330 °C. The SiO_x/Si intensity ratio increased by 0.14 upon a 0.5-nm Al_2O_3 deposition, and it subsequently varied by only 0.02–0.03 throughout the processing steps (Fig. S6, black columns). The position of the SiO_x shoulder shifted to lower binding energies (larger SiO/Si_2O_3 fraction) after five cycles of Al_2O_3 deposition. While the GeO_x 3d and 2p components also shifted to lower binding energies, they slightly decreased upon Al_2O_3 deposition. Furthermore, the GeO_x/Ge3d was significantly reduced by UHV annealing and atomic H dosing (Fig. S6, red columns). The

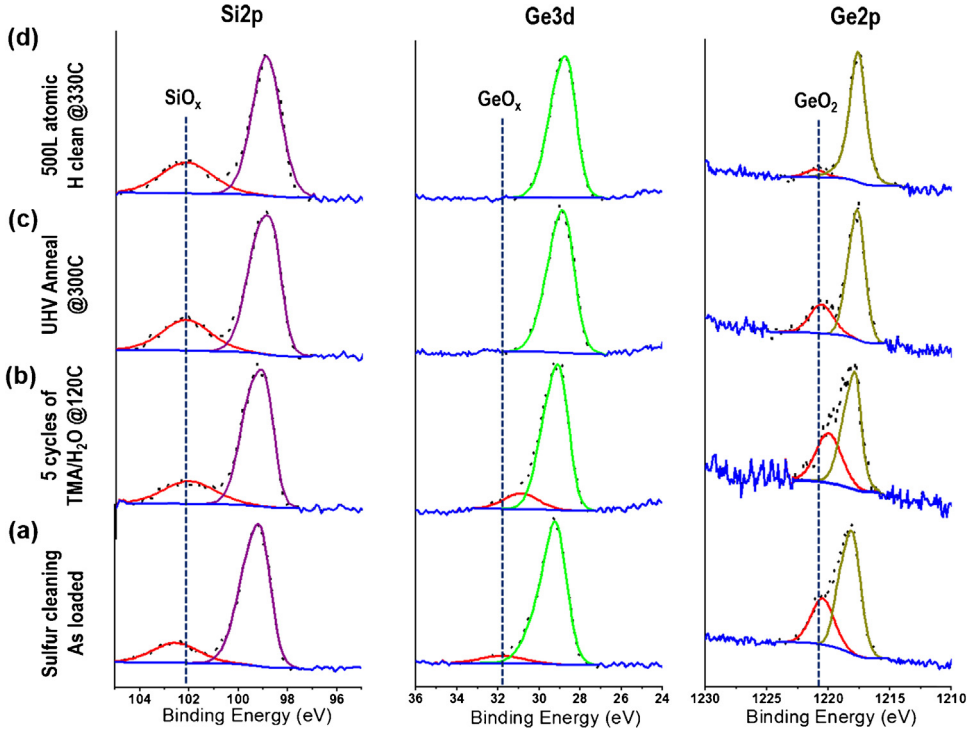

Fig. 8. Si2p, Ge3d, and Ge2p spectra for S-passivated (a) as-loaded, (b) after five cycles of TMA and an H_2O dose (b), (c) UHV annealing at 300 °C, and (d) 500 L of an atomic H dose at 330 °C.

simultaneous reduction in GeOx/Ge and the increase in SiOx/Si are consistent with the oxygen exchange from the Ge to Si surface atoms due to a higher thermal stability of the Si—O bonds than Ge—O at temperatures as high as 300 °C [34]. There was also a relatively large GeO_2 peak in the Ge2p spectra that shifted to lower binding energies after Al_2O_3 deposition. However, after UHV annealing, it shifted back to its original binding energy, despite a reduction in its intensity. After annealing at 300 °C, the GeO_2 is only observed in the surface-sensitive Ge2p signal and not in the bulk sensitive Ge3d spectra. As the EAL for Ge2p is 0.55 nm, which is comparable to the Al_2O_3 thickness (0.5–0.7 nm), this GeO_2 component is likely to be localized at the interface, within or on top of the oxide. A substantial surface component is consistent with the Ge2p AR-XPS spectra in Fig. 7e, where a large GeO_2 peak is observed at large grazing angles.

S passivation on Ge and many of the III-V surfaces causes the formation of surface —S bonds [35,36]. To determine the bonding state and surface coverage of S atoms, S2p peaks were measured by XPS at a 30° take-off angle for the four different processing steps in Fig. 8, as shown in Fig. 9a. There is residual S on the as-loaded sample surface, as well as at the Al_2O_3/SiGe interface after ALD, UHV annealing, and atomic H cleaning. Using the Beer–Lambert attenuation equation for photoelectrons, assuming that the SiGe monolayer is 0.15-nm thick [37], the S surface coverage has been estimated for the as-loaded sample as 0.54 ML, where ML is the fraction of a layer. As Si and Ge bond strongly to S [38], it is possible that S is bonded to the surface with single —SH bonds (Ge—SH and Si—SH) or bridge bonds (Ge—S—Ge, Si—S—Si, etc.). As S passivation resulted in improved insulating properties and nucleation densities both for 120 and 300 °C processing temperatures, it can be hypothesized that the majority of surface S termination is —SH; —SH is polar and negative partial charge on S atoms should electrostatically interact with the positively charged Al atoms in TMA, similar to —OH termination [39]. S coverage was reduced after Al_2O_3 ALD,

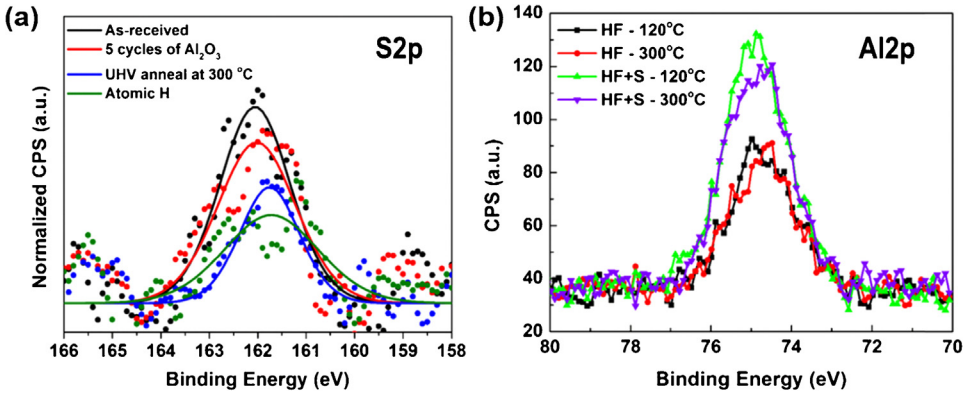

Fig. 9. (a) S2p peaks from in situ XPS for various processing steps on the sample surface showing a very small amount of S. The S2p signal is normalized to the sum of the peak heights for Si2p and Ge3d. (b) The Al2p peak from the AR-XPS measurements at the take-off angle of 64.25°, showing the higher intensity of Al and therefore the nucleation density of Al_2O_3 on S-passivated SiGe surfaces compared to HF-treated surfaces.

UHV annealing, and atomic H to 0.35 ML, 0.26 ML, and 0.23 ML, respectively. Therefore, it is possible that after full forming gas annealing at typical MOSCAP processing pressures, the majority of the interfacial S is removed. The remaining S could be incorporated into the Al_2O_3–SiGe interface in the form of Ge—S—Al interfacial bonds [39,40].

To understand how surface treatment affects the nucleation density of Al_2O_3 on SiGe surfaces, the AR-XPS intensity of the Al was determined after eight ALD cycles. Fig. 9b shows the Al2p peaks on HF-treated and S-passivated surfaces after 0.8 nm of Al_2O_3 deposition at 120, 200, and 300 °C. These peaks were measured by AR-XPS at the take-off angle of 64.25°. S passivation resulted in at least a twice-larger Al2p intensity, consistent with the better nucleation density of Al_2O_3 on the SiGe(0 0 1) surfaces. In addition, the Al_2O_3 thickness estimation using the intensity vs. take-off angle fitting of Si2p and Al2s peaks (Table S1) showed a 0.14-nm thicker oxide on S-passivated surfaces than HF-treated surfaces, which is in agreement with the larger initial growth rate as a result of S passivation. This thickness difference decreases through the deposition of a larger number of cycles and is expected to be negligible beyond 25 or 30 cycles of ALD. Therefore, S passivation is expected to result in a higher nucleation density and lower density of pinholes near the interface, which is consistent with an order-of-magnitude smaller gate leakage current for its MOSCAPs [41].

4. Conclusion

It has been shown that in the absence of S passivation, a lower ALD temperature results in a higher Al_2O_3–SiGe interface quality and lower gate oxide leakage for H-terminated SiGe. By applying ex situ S passivation using $(NH_4)_2S$, a much weaker dependence of interface quality and leakage current on the ALD temperature was observed. In addition, S passivation resulted in greater air stability of the cleaned surface against ambient oxidation. Specifically, for up to an hour of air exposure, V_{FB} was maintained in the same range as the sample with no air exposure, showing the capability of this passivation in extending the device fabrication queue time. XPS measurements revealed that S passivation removes a large amount of Ge—O bonds at the Al_2O_3–SiGe interface, leading to direct bonding between them via Al—O—Si. Moreover, S passivation led to a higher nucleation density consistent with an order-of-magnitude smaller leakage current compared to H-terminated samples.

Acknowledgements

The authors would like to thank Dr. Bernd Fruhberger, Larry Grissom, Ivan Harris, and Sean Park of UCSD Calit2 for their assistance with ALD and metal deposition at the UCSD Nano3 cleanroom facility. SiGe wafers were provided by Applied Materials Inc. This work is partially supported by SRC-GRC Task 2451.001 and by a gift from Applied Materials Inc.

Appendix A. Supplementary data

Supplementary data associated with this article can be found, in the online version, at http://dx.doi.org/10.1016/j.apsusc.2016.01.123.

References

[1] C.W. Liu, M. Ostling, J.B. Hannon, New materials for post-Si computing, MRS Bull. 39 (2014) 658–662.
[2] H. Riel, L.E. Wernersson, M.W. Hong, J.A. del Alamo, III-V compound semiconductor transistors-from planar to nanowire structures, MRS Bull. 39 (2014) 668–677.
[3] D.V. Lang, R. People, J.C. Bean, A.M. Sergent, Measurement of the band-gap of Gexsi1-X/Si strained-layer heterostructures, Appl. Phys. Lett. 47 (1985) 1333–1335.
[4] J.D. Cressler, SiGe HBT technology: a new contender for Si-based RF and microwave circuit applications, IEEE Trans. Microw. Theory 46 (1998) 572–589.
[5] H. Shang, M.M. Frank, E.P. Gusev, J.O. Chu, S.W. Bedell, K.W. Guarini, M. Ieong, Germanium channel MOSFETs: opportunities and challenges, IBM J. Res. Dev. 50 (2006) 377–386.
[6] N. Lu, W. Bai, A. Ramirez, C. Mouli, A. Ritenour, M.L. Lee, D. Antoniadis, D.L. Kwong, Ge diffusion in Ge metal oxide semiconductor with chemical vapor deposition HfO_2 dielectric, Appl. Phys. Lett. 87 (2005).
[7] R.L. Xie, C.X. Zhu, Effects of sulfur passivation on germanium MOS capacitors with HfON gate dielectric, IEEE Electron Device Lett. 28 (2007) 976–979.
[8] S. Sioncke, H.C. Lin, L. Nyns, G. Brammertz, A. Delabie, T. Conard, A. Franquet, J. Rip, H. Struyf, S. De Gendt, M. Muller, B. Beckhoff, M. Caymax, S-passivation of the Ge gate stack: tuning the gate stack properties by changing the atomic layer deposition oxidant precursor, J. Appl. Phys. 110 (2011).
[9] D. Shahrjerdi, E. Tutuc, S.K. Banerjee, Impact of surface chemical treatment on capacitance-voltage characteristics of GaAs metal–oxide–semiconductor capacitors with Al_2O_3 gate dielectric, Appl. Phys. Lett. 91 (2007).
[10] N. Goel, P. Majhi, C.O. Chui, W. Tsai, D. Choi, J.S. Harris, InGaAs metal–oxide–semiconductor capacitors with HfO_2 gate dielectric grown by atomic-layer deposition, Appl. Phys. Lett. 89 (2006).
[11] A.J. Kerr, E. Chagarov, S. Gu, T. Kaufman-Osborn, S. Madisetti, J. Wu, P.M. Asbeck, S. Oktyabrsky, A.C. Kummel, Preparation of gallium nitride surfaces for atomic layer deposition of aluminum oxide, J. Chem. Phys. 141 (2014).
[12] M. Houssa, D. Nelis, D. Hellin, G. Pourtois, T. Conard, K. Paredis, K. Vanormelingen, A. Vantomme, M.K. Van Bael, J. Mullens, M. Caymax, M. Meuris, M.M. Heyns, H_2S exposure of a (1 0 0)Ge surface: Evidences for a (2×1) electrically passivated surface, Appl. Phys. Lett. 90 (2007).
[13] S. Sioncke, H.C. Lin, G. Brammertz, A. Delabie, T. Conard, A. Franquet, M. Meuris, H. Struyf, S. De Gendt, M. Heyns, C. Fleischmann, K. Temst, A. Vantomme, M. Muller, M. Kolbe, B. Beckhoff, M. Caymax, Atomic layer deposition of high-kappa dielectrics on sulphur-passivated germanium, J. Electrochem. Soc. 158 (2011) H687–H692.
[14] C. Fleischmann, M. Houssa, M. Muller, B. Beckhoff, H.G. Boyen, M. Meuris, K. Temst, A. Vantomme, Liquid-phase adsorption of sulfur on germanium: reaction mechanism and atomic geometry, J. Phys. Chem. C 117 (2013) 7451–7458.
[15] H.P. Chen, Y. Yuan, B. Yu, J. Ahn, P.C. McIntyre, P.M. Asbeck, M.J.W. Rodwell, Y. Taur, Interface-state modeling of Al_2O_3–InGaAs MOS from depletion to inversion, IEEE Trans. Electron Devices 59 (2012) 2383–2389.
[16] Y. Yuan, B. Yu, J. Ahn, P.C. McIntyre, P.M. Asbeck, M.J.W. Rodwell, Y. Taur, A distributed bulk-oxide trap model for Al_2O_3 InGaAs MOS devices, IEEE Trans Electron Devices 59 (2012) 2100–2106.
[17] Y.C. Byun, S. Choi, Y. An, P.C. McIntyre, H. Kim, Tailoring the interface quality between HfO_2 and GaAs via in situ ZnO passivation using atomic layer deposition, ACS Appl. Mater. Interfaces 6 (2014) 10482–10488.
[18] K. Martens, C.O. Chui, G. Brammertz, B. De Jaeger, D. Kuzum, M. Meuris, M.M. Heyns, T. Krishnamohan, K. Saraswat, H.E. Maes, G. Groeseneken, On the correct extraction of interface trap density of MOS devices with high-mobility semiconductor substrates, IEEE Trans. Electron Devices 55 (2008) 547–556.
[19] E.H. Poindexter, G.J. Gerardi, M. Rueckel, P.J. Caplan, Electronic traps and P_b centers at the Si/SiO_2 interface: band-gap energy distribution, J. Appl. Phys. 56 (1984) 2844–2849.
[20] M.J. Uren, J.H. Stathis, E. Cartier, Conductance measurements on P_b centers at the (1 1 1) $Si:SiO_2$ interface, J. Appl. Phys. 80 (1996) 3915–3922.
[21] P.K. Hurley, B.J. O'Sullivan, F.N. Cubaynes, P.A. Stolk, F.P. Widdershoven, J.H. Das, Examination of the Si(1 1 1)–SiO_2, Si(1 1 0)–SiO_2, and Si(1 0 0)–SiO_2 interfacial properties following rapid thermal annealing, J. Electrochem. Soc. 149 (2002) 194–197.
[22] N.H. Thoan, K. Keunen, V.V. Afanas'ev, A. Stesmans, Interface state energy distribution and P_b defects at Si(1 1 0)/SiO_2 interfaces: comparison to (1 1 1) and (1 0 0) silicon orientations, J. Appl. Phys. 109 (2011).
[23] P. Masson, J.L. Autran, M. Houssa, X. Garros, C. Leroux, Frequency characterization and modeling of interface traps in $HfSi_xO_y/HfO_2$ gate dielectric stack from a capacitance point-of-view, Appl. Phys. Lett. 81 (2002) 3392–3394.
[24] G.J. Gerardi, E.H. Poindexter, M.E. Rueckel, P.J. Caplan, Interface traps and P_b centers in oxidized (1 0 0) silicon wafers, Appl. Phys. Lett. 49 (1986) 348–350.
[25] J. Robertson, High dielectric constant gate oxides for metal oxide Si transistors, Rep. Prog. Phys. 69 (2006) 327–396.
[26] J.W. Fowler, G.L. Hogg, D.T. Phillips, Control of multiproduct bulk server diffusion/oxidation processes. Part 2: Multiple servers, IIE Trans. 32 (2000) 167–176.
[27] Y. Taur, T.H. Ning, Fundamentals of Modern VLSI Devices, Second ed., Cambridge University Press, Cambridge/New York, 2009.
[28] F.J. Himpsel, F.R. Mcfeely, A. Talebibrahimi, J.A. Yarmoff, G. Hollinger, Microscopic structure of the SiO_2/Si interface, Phys. Rev. B 38 (1988) 6084–6096.
[29] K. Prabhakaran, T. Ogino, Oxidation of Ge(1 0 0) and Ge(1 1 1) surfaces: an Ups and Xps study, Surf. Sci. 325 (1995) 263–271.
[30] C.J. Powell, A. Jablonski, F. Salvat, NIST databases with electron elastic-scattering cross sections, inelastic mean free paths, and effective attenuation lengths, Surf. Interface Anal. 37 (2005) 1068–1071.

[31] G.K. Dalapati, S. Chattopadhyay, K.S.K. Kwa, S.H. Olsen, Y.L. Tsang, R. Agaiby, A.G. O'Neill, P. Dobrosz, S.J. Bull, Impact of strained-Si thickness and Ge out-diffusion on gate oxide quality for strained-Si surface channel n-MOSFETs, IEEE Trans. Electron Devices 53 (2006) 1142–1152.
[32] W.C. Hua, M.H. Lee, P.S. Chen, S. Maikap, C.W. Liu, K.M. Chen, Ge outdiffusion effect on flicker noise in strained-Si nMOSFETs, IEEE Electron Device Lett. 25 (2004) 693–695.
[33] M. Zielinski, R. Wojcieszak, S. Monteverdi, M. Mercy, M.M. Bettahar, Hydrogen storage in nickel catalysts supported on activated carbon, Int. J. Hydrog. Energy 32 (2007) 1024–1032.
[34] T. Kaufman-Osborn, E.A. Chagarov, S.W. Park, B. Sahu, S. Siddiqui, A.C. Kummel, Atomic imaging and modeling of passivation, functionalization, and atomic layer deposition nucleation of the SiGe(0 0 1) surface via H_2O_2(g) and trimethylaluminum dosing, Surf. Sci. 630 (2014) 273–279.
[35] C. Fleischmann, S. Sioncke, S. Couet, K. Schouteden, B. Beckhoff, M. Muller, P. Honicke, M. Kolbe, C. Van Haesendonck, M. Meuris, K. Temst, A. Vantomme, Towards passivation of Ge(1 0 0) surfaces by sulfur adsorption from a (NH4)(2)S solution: a combined NEXAFS, STM and LEED study, J. Electrochem. Soc. 158 (2011) H589–H594.
[36] Z.H. Lu, D. Landheer, J.M. Baribeau, L.J. Huang, W.W. Lau, Si/Ge/S multilayer passivation of GaAs(1 0 0) for metal–insulator–semiconductor capacitors, Appl. Phys. Lett. 64 (1994) 1702–1704.
[37] P. Schittenhelm, M. Gail, G. Abstreiter, Self-organized MBE growth of Ge-rich SiGe dots on Si(1 0 0), J. Cryst. Growth 157 (1995) 260–264.
[38] Y.-R. Luo, Y.-R. Luo, Comprehensive Handbook of Chemical Bond Energies, CRC Press, Boca Raton, 2007.
[39] A. Delabie, S. Sioncke, S. Van Elshocht, M. Caymax, G. Pourtois, K. Pierloot, Chemisorption reaction mechanisms for atomic layer deposition of high-kappa oxides on high mobility channels, At. Layer Depos. Appl. 6 (33) (2010) 343–353.
[40] A. Delabie, S. Sioncke, J. Rip, S. Van Elshocht, M. Caymax, G. Pourtois, K. Pierloot, Mechanisms for the trimethylaluminum reaction in aluminum oxide atomic layer deposition on sulfur passivated germanium, J. Phys. Chem. C 115 (2011) 17523–17532.
[41] M. Depas, R.L. Vanmeirhaeghe, W.H. Laflere, F. Cardon, Electrical characteristics of Al/SiO_2/N-Si tunnel-diodes with an oxide layer grown by rapid thermal-oxidation, Solid State Electron. 37 (1994) 433–441.